Journal of Rare Earths 39 (2021) 43–50

Contents lists available at ScienceDirect

Journal of Rare Earths

journal homepage: http://www.journals.elsevier.com/journal-of-rare-earths

Effect of tungsten oxide on ceria nanorods to support copper species as CO oxidation catalysts☆

Yu'nan Li [a], Lin Gan [a,*], Rui Si [b,**]

[a] Hubei Collaborative Innovation Center for Advanced Organic Chemical Materials, Ministry of Education Key Laboratory for the Green Preparation and Application of Functional Materials and School of Material Science and Engineering, Hubei University, Wuhan 430062, China
[b] Zhangjiang Laboratory, Shanghai Synchrotron Radiation Facility, Shanghai 201204, China

ARTICLE INFO

Article history:
Received 24 September 2019
Received in revised form
30 November 2019
Accepted 31 December 2019
Available online 7 January 2020

Keywords:
Copper catalyst
Ceria
Tungsten oxide
CO oxidation
Structure-activity relationship
Rare earths

ABSTRACT

In this work, tungsten oxide with different concentrations (0, 0.4 at%, 2.0 at% and 3.2 at%) was introduced to the ceria nanorods via a deposition-precipitation (DP) approach, and copper species of *ca.* 10 at% were sequentially anchored onto the modified ceria support by a similar DP route. The aim of the study was to investigate the effect of the amount of tungsten oxide (0, 0.4 at%, 2.0 at%, and 3.2 at%) modifier on the copper-ceria catalysts for CO oxidation reaction and shed light on the structure-activity relationship. By the aids of multiple characterization techniques including N_2 adsorption, high-resolution transmission electron microscopy (HRTEM), powder X-ray diffraction (XRD), X-ray absorption fine structure (XAFS), and temperature-programmed reduction by hydrogen (H_2-TPR) in combination with the catalytic performance for CO oxidation reaction, it is found that the copper-ceria samples maintain the crystal structure of the fluorite *fcc* CeO_2 phase with the same nanorod-like morphology with the introduction of tungsten oxide, while the textural properties (the surface area, pore volume and pore size) of ceria support and copper-ceria catalysts are changed, and the oxidation states of copper and tungsten are kept the same as Cu^{2+} and W^{6+} before and after the reaction, but the introduction of tungsten oxide (WO_3) significantly changes the metal-support interaction (transfer the CuO_x clusters to Cu-[O_x]-Ce species), which delivers to impair the catalytic activity of copper-ceria catalysts for CO oxidation reaction.

© 2021 Chinese Society of Rare Earths. Published by Elsevier B.V. All rights reserved.

1. Introduction

Nowadays, an increasing amount of carbon monoxide (CO) from industrial waste gas, automobile exhaust, and incomplete combustion of fossil fuel is being emitted into the atmosphere, which can cause serious safety and pollution problems.[1,2] An effective and convenient strategy to solve these problems is transforming CO into nontoxic CO_2 by appropriate catalytic processes. Hence, it is a great challenge to develop efficient catalysts with high activity and excellent stability. Up to now, oxide-supported noble metal (e.g., Au,[3] Pt[4] and Pd[5]) catalysts with extremely high activity for CO oxidation at relatively low temperature (lower than 80 °C, or even below room-temperature) have been intensively investigated. However, industrial applications of these catalytic materials are seriously hindered due to their high cost.[6–8] Therefore, it is necessary to exploit inexpensive non-noble metal catalysts with excellent reactivity for CO oxidation. Among them, copper was confirmed as a promising candidate. For example, alumina-supported CuMn bimetallic catalyst showed a high activity for CO oxidation with 100% conversion temperature as low as 120 °C.[9] Furthermore, $Cu/ZnO/Al_2O_3$ has been used industrially for methanol synthesis and water-gas shift reactions.[10,11]

Ceria (CeO_2), one of the most important functional rare-earth oxides, has attracted increasing international interest due to its excellent oxygen storage capacity and outstanding dispersibility of active metal species.[12–14] Nanoscaled ceria was reported as a superior support for CO oxidation and water-gas shift reactions, which can effectively improve the catalytic activity of the metal or metal oxide catalysts.[15–17] Corma et al. showed that the reactivity of CeO_2 supported catalysts is much better than that of TiO_2 or Fe_2O_3 matrix.[18] Among the various alternatives, copper-ceria catalysts have been intensively studied due to their features of low cost and high activity.[19] To further improve the catalytic properties, an

☆ **Foundation item:** Project supported by National Natural Science Foundation of China (21773288, 51902093) and National Key Basic Research Program of China (2017YFA0403402).
* Corresponding author.
** Corresponding author.
E-mail addresses: ganlin@hubu.edu.cn (L. Gan), sirui@sinap.ac.cn (R. Si).

https://doi.org/10.1016/j.jre.2019.12.015
1002-0721/© 2021 Chinese Society of Rare Earths. Published by Elsevier B.V. All rights reserved.

appropriate modification of ceria support was studied by many researchers. For instance, the addition of Zr into CuO-CeO_2 catalysts resulted in stronger synergistic interaction between copper and ceria, easier reducibility of active copper species and higher numbers of oxygen vacancies and active sites, which showed a significantly positive effect on the catalytic performance.[20–22] However, up to date, there is no available report on the effect of tungsten oxide (WO_x) on copper-ceria for the CO oxidation reaction, even the previous investigation showed that W–O–Ce originating from the interaction between WO_x and CeO_2 can promote the formation of oxygen vacancies and enhance the reducibility of ceria-supported metal/metal oxide catalysts.[23] Actually, tungsten oxide was usually added as a component modifier for the supports (SiO_2,[24] Al_2O_3,[25] etc.) of heterogeneous catalysts.

To obtain the reliable structure–activity relationship, advanced characterization techniques are required to precisely detect the complex structural properties of supported metal or metal oxide nanocatalysts. As for heterogeneous catalysis, X-ray absorption fine structure (XAFS) technique has been broadly applied to the analyses of the structural evolution of low-concentration active metal or metal oxide species. Particularly, X-ray near edge spectroscopy (XANES) and extended X-ray absorption fine structure (EXAFS) analyses are effective for the determination of both electronic structure (oxidation state, charge transfer, etc.) and local coordination structure (coordination number, bond distance, etc.) up to 0.6–0.8 nm, respectively.[26–30] On the other hand, temperature-programmed reduction by hydrogen (H_2-TPR), which is a conventional catalytic approach, and plays key role in the investigation of the reducibility and metal-support interaction of the supported catalysts.[31] Previously, by using XANES/EXAFS and H_2-TPR, Wang et al. determined that the highly dispersed CuO_x, other than the Cu-[O_x]-Ce structure, were the crucial active species for the preferential oxidation of CO reaction.[32]

Therefore, in this work, ceria nanorods were used as the oxide support to anchor copper species, and the support was modified by introducing low-concentration tungsten oxide via a DP approach. With the help of multiple characterization methods including N_2 adsorption, XAFS, and H_2-TPR, the effects of tungsten oxide on copper-ceria catalysts for CO oxidation reaction were studied in detail, in order to correlate the catalytic activity with the structure of certain copper species and their interaction between the metal-support to investigate the structure-activity relationship on these copper-ceria catalysts. It is found that the introduction of tungsten oxide (WO_3) significantly changes the metal-support interaction in Cu–Ce–O, which delivers to change the catalytic performance of copper-ceria catalysts for CO oxidation. The study results are expected to give guidelines for modification of CeO_2 and will attract a broad readership of copper-ceria catalysts for CO oxidation reaction.

2. Experimental

2.1. Catalyst preparation

All the chemicals used in this work were of analytical grade and purchased from Sinopharm Chemical Reagent Co., Ltd. without any further purification.

The ceria nanorods were synthesized by a hydrothermal method. $Ce(NO_3)_3{\cdot}6H_2O$ (3 mmol) was added into an aqueous NaOH (6 mol/L, 60 ml) solution with vigorous stirring for about 30 min. After the precipitation process, the stock solution was transferred into a Teflon bottle (inner volume: 100 mL), and further tightly sealed in a stainless-steel autoclave. The hydrothermal procedure was carried out in a temperature-controlled electric oven at 100 °C for 24 h. Then, the precipitates were washed by Millipore (>18 MΩ) water for four times and by ethanol for once. The ceria nanorods was obtained by drying the as-washed product under vacuum at 80 °C for 12 h and further calcined in air at 400 °C for 4 h (heating rate: 2 °C/min).

Tungsten oxide-modified ceria nanorods were synthesized via a deposition-precipitation (DP) method. Typically, 1 g of as-calcined ceria nanorods were suspended in 50 mL Millipore water. After stirring for 15 min, ammonium carbonate solution (25 mL, 1 mol/L) was added. Ammonium metatungstate ($H_{42}N_{10}O_{42}W_{12}O_{40}$, 0.0049 mmol) was dissolved in 25 mL Millipore water, and then added into the above stock solution dropwise. After stirring and aging at room temperature for 1 h, the as-formed precipitates were filtrated and then were washed by Millipore water. The as-washed powders were dried under vacuum at 80 °C overnight and further calcined in air at 400 °C for 4 h (heating rate: 2 °C/min). The as-calcined tungsten oxide-modified ceria nanorods were denoted as W_xCe (x is the molar ratio of W/Ce).

Copper catalysts supported on tungsten oxide-modified ceria nanorods were also synthesized via a DP approach. Specifically, copper nitrate ($Cu(NO_3)_2{\cdot}3H_2O$, 0.1543 g) and the as-calcined $W_{0.4}Ce$ (1 g) were dissolved or suspended in 100 mL Millipore water by vigorous stirring. Then, Na_2CO_3 aqueous solution (0.5 mol/L) was dropped into the above mentioned solution until the pH value reached 9. After stirring and aging at 80 °C for another 3 h, the as-obtained precipitates were gathered by filtration and then washed with Millipore water for three times. The as-washed powders were dried under vacuum at 80 °C overnight and then calcined in air at 400 °C for 4 h (heating rate: 2 °C/min). The as-calcined copper catalysts supported on tungsten oxide-modified ceria nanorods were denoted as Cu_yW_xCe (x and y are the molar ratios of W/Ce and Cu/Ce, respectively).

2.2. Characterization

The experimental ratios of Cu/W/Ce were determined by inductively coupled plasma atomic emission spectroscopy (ICP-AES) on an IRIS Intrepid II XSP instrument (Thermo Electron Corporation).

The nitrogen adsorption-desorption characterization was analyzed on an ASAP2020-HD88 analyzer (Micromeritics Co., Ltd.) at 77 K. The measured powders were degassed at 250 °C under vacuum (<100 μm Hg) for over 4 h before the introduction of N_2. The pore-size (r_p) distribution of each sample was calculated according to the desorption branch of the obtained isotherms with the BJH method. The BET specific surface areas (S_{BET}) were calculated from the data between 0.05 and 0.20 relative pressure.

The powder X-ray diffraction (XRD) patterns were obtained on a Bruker D8 Advance diffractometer (40 kV and 40 mA) or a Malvern Panalytical X Pert powder diffractometer (40 kV and 40 mA), using Cu Kα1 radiation ($\lambda = 0.15406$ nm) with a scanning rate of 4 °C/min. The 2θ angles were calibrated with a μm-scale alumina (α-Al_2O_3) standard. The diffraction patterns were gathered from 10° to 90° with a step of 0.02°. The ground sample was planished on a quartz sample holder before each test. Cell dimensions of cubic CeO_2 were obtained from the corresponding powder data with a "LAPOD" software of least-squares refinement by the Cohen's method.[33,34]

The transmission electron microscopy (TEM) and high-resolution TEM (HRTEM) images were obtained from an FEI Tecnai G2 F20 microscope (200 kV). The measured samples were ultrasonic dispersed in absolute alcohol for 5 min, and then placed a drop of liquid supernatant on an ultra-thin (3–5 nm) carbon film-coated Mo grid. The sample grid was dried naturally under dark conditions before inserted into the sample holder.

The X-ray absorption fine structure (XAFS) spectroscopy at the Cu K (E_0 = 8979 eV) edge and W L_3 (E_0 = 10207 eV) edge was

operated at the BL14W1 beamline of Shanghai Synchrotron Radiation Facility (SSRF) at 3.5 GeV in "top-up" mode with a constant current of 240 mA. The XAFS spectra of Cu K edge and W L_3 edge were recorded in transmission mode and fluorescence mode with a Lytle ion chamber, respectively. The X-ray energy was calibrated with the absorption edge of pure Cu foil and W foil, respectively. Athena and Artemis codes were used to extract the data and fit the profiles. For the X-ray absorption near edge structure (XANES) part, the experimental absorption coefficients as a function of energies $\mu(E)$ were processed by background subtraction and normalization procedures, and reported as "normalized absorption". The chemical valences of Cu and W were determined with the linear combination fit by comparison to the corresponding references of Cu/CuO/Cu_2O and W/WO_3 based on the normalized XANES profiles in the Athena software. For the extended X-ray absorption fine structure (EXAFS) part, the Fourier transformed (FT) data in *R* space were analyzed by applying the first shell approximation model for Cu–O and W–O contributions. The passive electron factors S_0^2 were determined by fitting the experimental data on Cu foil and W foil and fixing the coordination number (CN) of Cu–Cu and W–W to be 12, and then fixed for further analyses of the measured samples. The parameters describing the electronic structure such as correction to the photoelectron energy origin E_0 and local coordination structure including CN, bond distance (*R*) and Debye-Waller (D.W.) factor around the absorbing atoms could be varied during the fitting process. The fitted ranges for *k* and *R* spaces were selected to be $k = 20–109\ nm^{-1}$ with $R = 0.10–0.19$ (Cu–O) nm (k^3 weighted) and $k = 20–11.9\ nm^{-1}$ with $R = 0.11–0.21$ (W–O) nm (k^3 weighted), respectively.

2.3. Catalytic tests

The temperature-programmed reduction by hydrogen (H_2-TPR) was conducted in a Micromeritics Auto Chem II (Micromeritics Co., Ltd., US) equipped with a thermal conductivity detector (TCD). The 50 mg laminar and sieved (40–60 mesh) powders were pretreated in O_2 (5%O_2/He) at 300 °C for 30 min, and then cooled down naturally to room temperature before reduction. The reduction process was performed with a gas mixture of 5% H_2/N_2 (99.997% purity, Shanghai Weichuang Co., China) from room temperature to 800 °C (flow rate: 50 mL/min; heating rate: 10 °C/min).

The CO oxidation activities of the copper-catalysts supported on tungsten oxide-modified ceria nanorods were estimated in a Micromeritics Auto Chem II (Micromeritics Co., Ltd., US). The 25 mg of sieved (40–60 mesh) powders were pre-oxidized (5%O_2/He) at 300 °C for 30 min before each test. After cooling down to room temperature in the same pretreated atmosphere, the tested sample was then switched to pure He for another 5 min. For the CO oxidation reaction, a gas mixture of 2%CO/1%O_2/97%He (99.997% purity, Shanghai Weichuang Co., China) passed through the catalysts at a flow rate of 50 mL/min, corresponding to a space velocity of 120000 mL/(h·g_{cat}). The variations of CO and CO_2 were monitored by a micro gas chromatography (GC) (INFICON Co., Ltd., United States) in outlets. The CO conversion ($CO_{conv.}$) was calculated accordingly to the following equation: $CO_{conv} = (CO_{in}–CO_{out})/CO_{in} \times 100\%$.

3. Results and discussion

In this work, the copper catalysts supported on tungsten oxide-modified ceria nanorods were prepared via a two-step sequential deposition-precipitation method. Table 1 shows the experimental loadings of copper and tungsten, determined by ICP-AES. It can be seen that the copper concentrations (7.8 at%–10 at%) are close to that of the designed value (10 at%) whether with or without the addition of W, identifying the successful deposition of Cu during the synthesis process. However, there is a severe deviation in the tungsten concentrations between the theoretical values (1.0 at%, 5.0 at%, and 15.0 at%) and the measured levels (0.4 at%, 2.0 at%, and 3.2 at%), resulting in 60%–80% loss of W during the applied DP process (see Table 1). This could be due to the ineffective precipitation of W^{6+} ion from the tungsten precursor and/or the formation of soluble tungsten-ammonia complex during the DP process.

Table 1
Metal ratios of Cu/W/Ce ($C_{Cu/W/Ce}$), BET Specific surface areas (S_{BET}), BJH pore volume (V_p), lattice constants (*a*) of CeO_2 and average particle sizes calculated from XRD (D_{XRD}) or TEM (D_{TEM}) for copper catalysts supported on tungsten oxide-modified ceria nanorods.

Sample	$C_{Cu/W/Ce}$ [a] (at%)	S_{BET} [b] (m^2/g)	V_P [b] (cm^3/g)	*a* [c] (nm)	D_{XRD} [c] (nm)	D_{TEM} [e] (nm)
CeO_2	–	122	0.57	0.54039 (7)	12	8.1 ± 1.4
$W_{0.4}Ce$	–	120	0.44	0.54033 (3)	12	–
$W_{2.0}Ce$	–	123	0.45	0.53908 (9)	11	–
$W_{3.2}Ce$	–	113	0.44	0.53947 (6)	11	–
CuCe	8.8/0/91.2	72	0.61	0.54051 (1) 0.54046 (7)[d]	12 12[d]	7.8 ± 1.2[d]
$CuW_{0.4}Ce$	10.0/0.4/89.6	114	0.40	0.54047 (9) 0.54034 (1)[d]	11 10[d]	–
$CuW_{2.0}Ce$	9.0/2.0/89.0	97	0.45	0.53975 (3) 0.53957 (9)[d]	12 11[d]	–
$CuW_{3.2}Ce$	7.8/3.2/89.0	110	0.46	0.54029 (2) 0.53992 (1)[d]	11 12[d]	8.0 ± 1.3[d]

[a] Determined by ICP-AES.
[b] Calculated from nitrogen adsorption-desorption results.
[c] Calculated from XRD patterns.
[d] Used after CO oxidation reaction.
[e] Average width statistic from TEM images.

Table 1 summaries the nitrogen adsorption results on the copper-ceria catalysts (CuCe and CuWCe), as well as the corresponding tungsten oxide-modified ceria supports (CeO_2 and WCe). It can be clearly seen that the BET specific surface areas of WCe (113–123 m^2/g) are in good agreement with that of pure CeO_2 (122 m^2/g), revealing that the addition of a small-amount tungsten does not modify the aggregation of primary grains of the ceria nanorods. However, for copper-containing samples, the S_{BET} values of CuWCe (97–114 m^2/g) are significantly larger than that of CuCe (72 m^2/g), indicating that the introduction of secondary tungsten oxide can well disperse the copper species onto ceria surface without partial coverage of pores. The related nitrogen adsorption/desorption isotherms and pore-size distribution histograms are shown in Fig. 1. Obviously, all the adsorption/desorption curves with or without the deposition of copper, can be assigned to type IV isotherm and the hysteresis loops in the p/p_0 range of 0.8–1.0 can be classified to type H3 (Fig. 1 (a) and (c)), which suggests that the materials consist of aggregated particles.[35] Interestingly, it shows that both CeO_2 and CuCe show slightly larger average pore diameters (Fig. 1 (b,d)) and higher BJH pore volumes (see Table 1) than those of the tungsten-modified samples (WCe and CuWCe). Therefore, it is confirmed that the introduction of secondary tungsten oxide into ceria nanorods increases the surface area for copper-ceria catalysts, while decreases the pore volume and the pore size for both ceria supports and copper-ceria catalysts.

CO oxidation reaction ($2CO + O_2 = 2CO_2$) with a space velocity as high as 120000 mL/(h·g_{cat}) was used to evaluate the catalytic performance of copper catalysts supported on tungsten oxide-modified ceria nanorods. The "light off" profiles in Fig. 2 (a) under transient mode display a high CO conversion. As a result of the fact that the "light off" temperatures for all the measured samples are narrow (*ca.* 60–120 °C), the stability tests on these preoxidized copper-ceria catalysts at 100 °C in 1%O_2/2%CO/97%He were carried out to enlarge the differences on CO oxidation reactivity. It can be

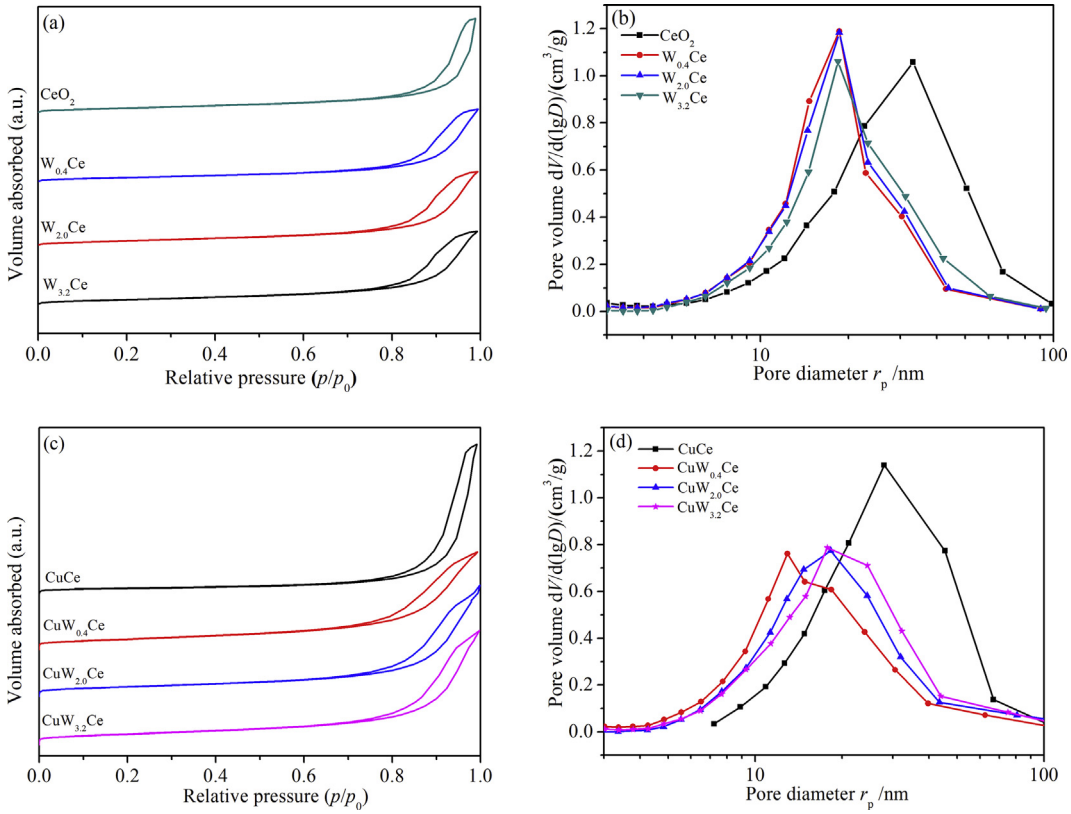

Fig. 1. N_2 adsorption experimental results of WCe (a, b) and CuWCe (c, d) samples. (a, c) Adsorption-desorption isotherm; (b, d) BJH pore-size distribution.

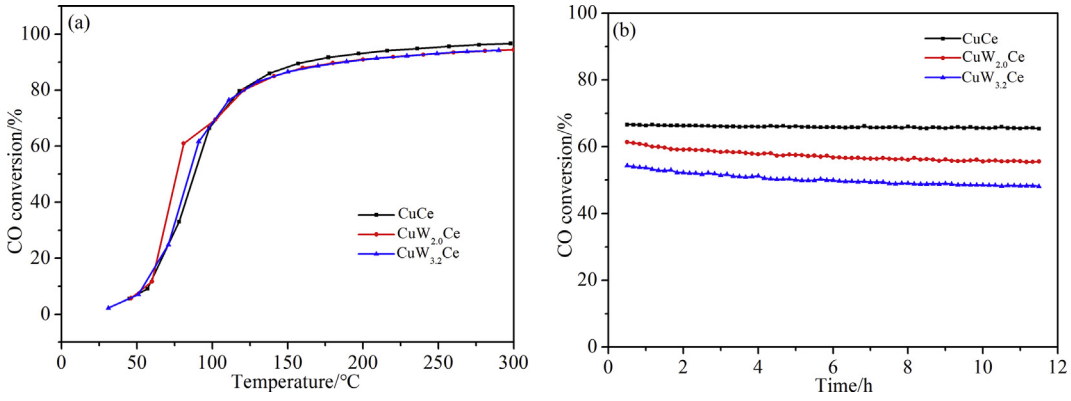

Fig. 2. "Light off" profiles (a) and stability results (b) at 100 °C on copper catalysts supported on tungsten oxide-modified ceria nanorods for CO oxidation reaction (2%CO/1%O_2/97% He, 120000 mL/(h·g_{cat})).

found from Fig. 2(b) that the CO conversions are nearly unchanged throughout the whole measurements up to 12 h, and the activity of each sample follows the sequence of CuCe > $CuW_{2.0}Ce$ > $CuW_{3.2}Ce$. This indicates that the introduction of tungsten oxide to the ceria nanorods has a negative effect, instead of positive contribution, on the catalytic performance of our copper catalysts.

XRD analyses were performed to determine the crystal structure of copper catalysts supported on tungsten oxide-modified ceria nanorods. The XRD patterns in Fig. 3 (a) indicates a fcc fluorite CeO_2 phase (JCPDS card No. 34-394) with lattice constants (a) of 0.53975–0.54051 nm (see Table 1) for all the fresh samples before the CO oxidation reaction. No peaks can be assigned to copper-containing (Cu/CuO/Cu_2O) or tungsten-involved (W/WO_2/WO_3) phase in both Cu/Ce and CuW/Ce samples, revealing that the deposited copper and tungsten species are either ultra-small in grain size and/or in very low concentration below the detection limit. Fig. 3(b) displays that the used catalysts after CO oxidation maintained the same CeO_2 phase as the fresh ones, verifying the good structural stability on the studied copper catalysts during the reaction up to 300 °C in 1%O_2/2%CO/97%He. The a values of ceria nanorods slightly decreases to 0.53957–0.54046 nm (see Table 1), indicating the removal of surface hydroxyls under the CO oxidation reaction conditions.[36]

TEM/HRTEM was used to observe the morphology of CeO_2 support. As shown in Fig. 4 (a, b), CeO_2 support is composed of nanorods with 20–110 nm in length and 8.1 ± 1.4 nm in width (also

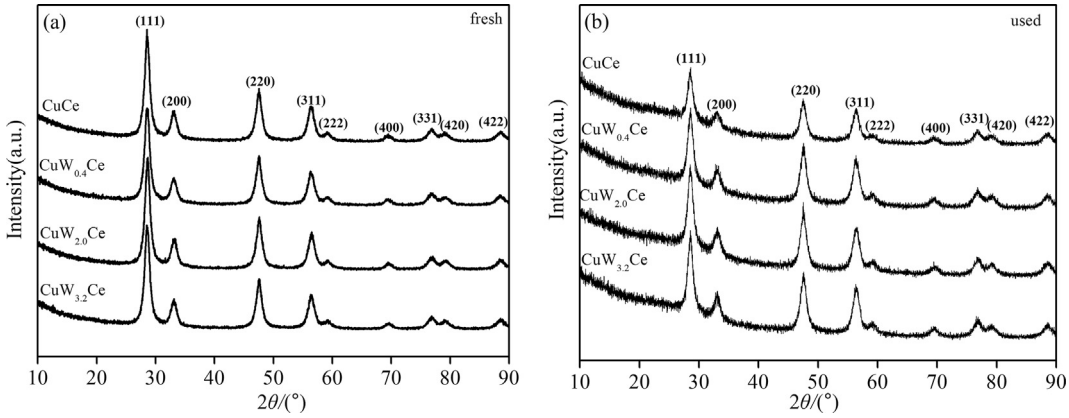

Fig. 3. XRD patterns of copper catalysts supported on tungsten oxide-modified ceria nanorods. (a) Fresh; (b) Used after CO oxidation reaction.

see Table 1). After the CO oxidation reaction, both CuCe and CuWCe catalysts show similar rod-like shape (Fig. 4 (c) and (d)) and close average width (see Table 1) for ceria. HRTEM images (Fig. 4(b–d)) clearly resolve an interplanar distance of 3.2 nm, which is corresponding to the (111) lattice fringes of CeO_2. The missing of any Cu- or W-containing component in HRTEM gives a hint that these copper and tungsten species are in ultra-small atoms or clusters on the surface of ceria nanorods, well consistent with the XRD results.

XANES analyses on Cu K and W L_3 edges were conducted to determine the oxidation states of copper and tungsten in different samples. With the help of various copper standards (Cu foil for Cu^0, Cu_2O for Cu^+ and CuO for Cu^{2+}), it can be concluded that fully oxidized copper (Cu^{2+}) species were identified in both fresh and used catalysts, whether with or without the addition of tungsten oxide (Fig. 5 (a) and Table 2). Similarly, by the aids of multiple tungsten references (W foil for W^0, WO_2 for W^{4+} and WO_3 for W^{6+}),

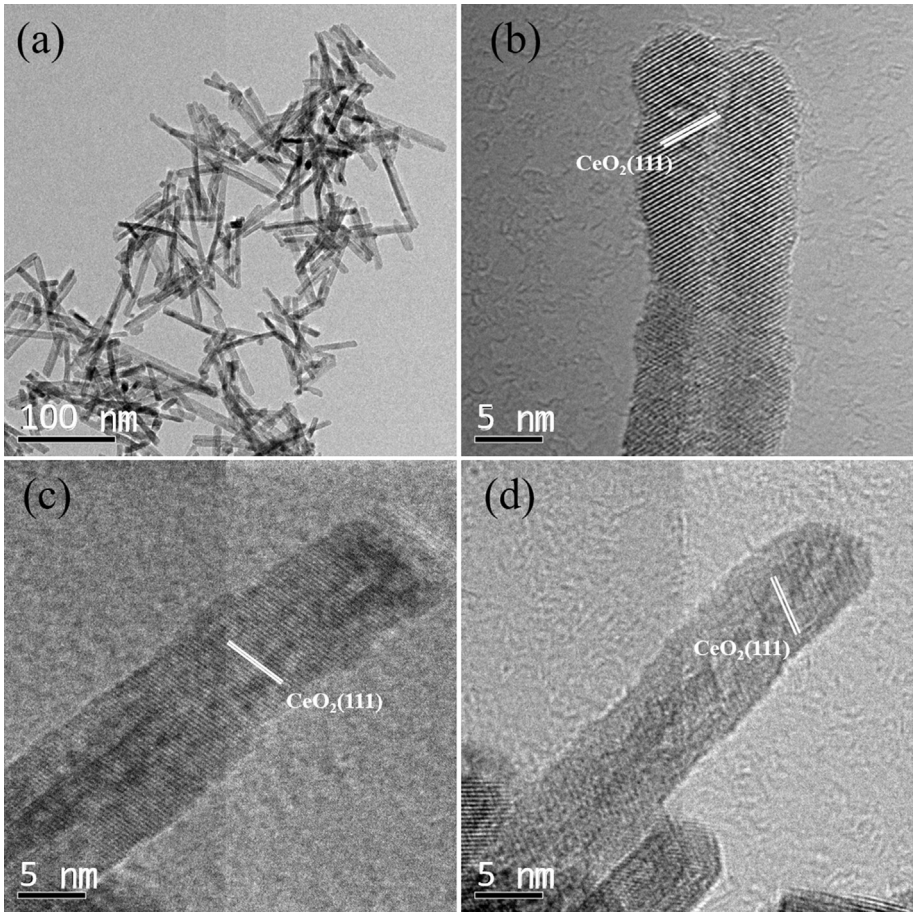

Fig. 4. TEM (a) and HRTEM (b–d) images of copper catalysts supported on tungsten oxide-modified ceria nanorods. (a, b) CeO_2; CuCe (c) and $CuW_{3.2}Ce$ (d) used after CO oxidation reaction.

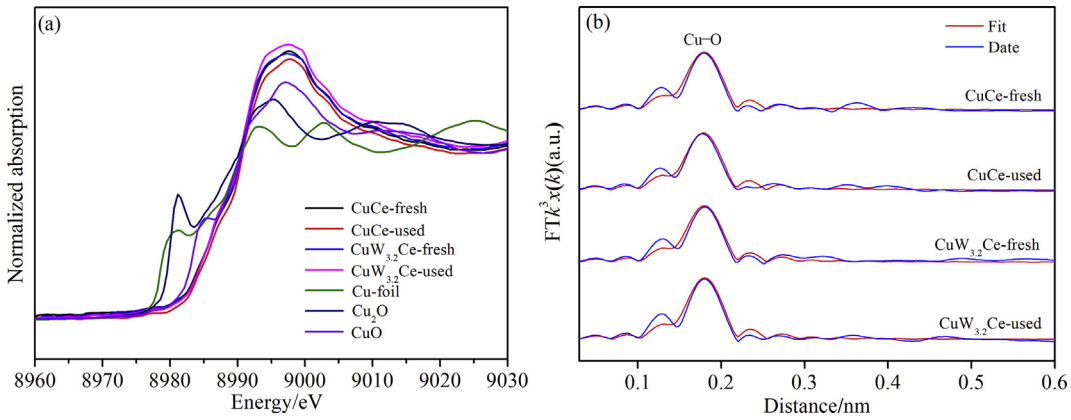

Fig. 5. XANES profiles (a) under and EXAFS spectra with fits in *R* space of Cu K edge (b) for copper catalysts supported on tungsten oxide-modified ceria nanorods.

Table 2
Averaged oxidation state of copper or tungsten (δ) and the corresponding EXAFS fitting results for Cu K and W L_3 edges (*R*: distance; CN: coordination number; σ^2: Debye-Waller factor; ΔE_0: inner potential correction) of copper catalysts supported on tungsten oxide-modified ceria nanorods.

Sample	δ[a]		Cu–O		W–O		σ^2	ΔE_0 (eV)
	Cu	W	*R* (nm)	CN	*R* (nm)	CN		
CuCe (fresh)	2.0	–	0.193 ± 0.001	3.7 ± 0.3	–	–	0.004 ± 0.001 (Cu–O)	8.8 ± 0.6 (Cu)
CuCe (used)	2.0	–	0.193 ± 0.001	3.7 ± 0.3	–	–	0.005 ± 0.002 (W–O)	6.4 ± 2.8 (W)
$CuW_{3.2}Ce$ (fresh)	2.0	6.0	0.194 ± 0.001	3.6 ± 0.3	0.175 ± 0.002	4.7 ± 1.1		
$CuW_{3.2}Ce$ (used)	2.0	6.0	0.194 ± 0.001	3.9 ± 0.3	0.177 ± 0.002	5.1 ± 1.1		

[a] Determined by linear combination analysis on the XANES profiles with references of Cu foil ($\delta = 0$)/CuO ($\delta = 2$) and W foil ($\delta = 0$)/WO_3 ($\delta = 6$) for Cu K and W L_3 edges, respectively.

the completely oxidized tungsten (W^{6+}) species, without any fraction of reduced components of W^0/W^{4+} were detected in all the investigated copper-ceria catalysts (Fig. 6(a) and Table 2). These results indicate that the reaction conditions (1%O_2/2%CO/97%He, up to 300 °C) still provided oxidation atmosphere on both CuCe and CuWCe samples. Furthermore, the profile mismatches of XANES on both Cu K and W L_3 edges between the copper-ceria catalysts supported on tungsten oxide-modified ceria nanorods and CuO/WO_3 in Figs. 5(a) and 6(a) reveal the totally different local coordination structures around Cu and W atoms in the studied samples.[37] However, it should be noted that the XANES analyses cannot distinguish the contributions from various Cu(II) components such as the crystallized CuO particles, the doped Cu^{2+} ions in ceria and the weakly/strongly bound surface CuO_x clusters.

The EXAFS fitting was carried out to reveal the local coordination structure around copper and tungsten centers in the samples. On the basis of EXAFS fitting results (Figs. 5 (b), 6 (b) and Table 2), it can be seen that a strong peak at $R = 0.194$ nm with CN of *ca.* 4 or $R = 0.175–0.177$ nm with CN of *ca.* 5 was identified for the first shell of Cu–O or W–O, respectively, which reveals the dominant oxidized Cu^{2+} or W^{6+} species in both fresh and used catalysts. Moreover, no direct metal–metal bonds (Cu–Cu and W–W) were determined, which is in good agreement with the XANES data. Furthermore, the copper species supported on either pure or tungsten oxide-modified ceria shows much weaker intensity of higher shells in the range of 0.3–0.4 nm (Fig. 5(b)), than the previous results on 5 wt%–10 wt% CuO-CeO_x catalysts before and after the preferential oxidation of CO,[38] which could be probably caused

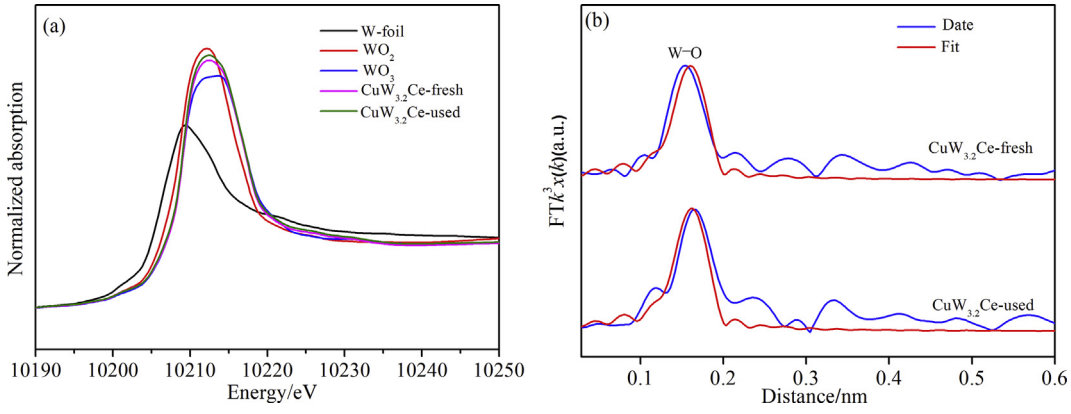

Fig. 6. XANES profiles (a) and EXAFS spectra with fits in *R* space of W L_3 edge (b) for copper catalysts supported on tungsten oxide-modified ceria nanorods.

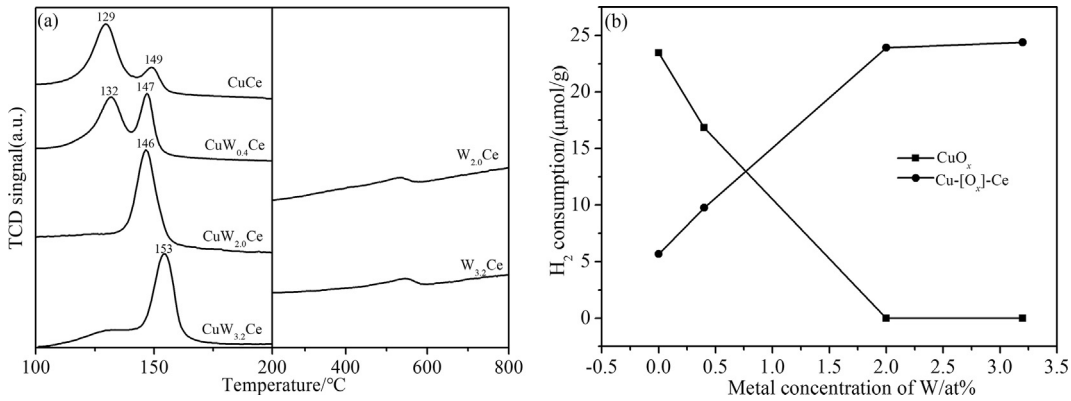

Fig. 7. H_2-TPR profiles (a) and deconvoluted H_2 consumption normalized by Cu weight vs metal concentration of W (b) for copper catalysts supported on tungsten oxide-modified ceria nanorods.

by the different aging conditions (Ref. 38: room-temperature, 1 h; this work: 80 °C, 3 h) during the deposition of copper in synthesis.

H_2-TPR was carried out to investigate the reducibility and metal-support interaction for the copper-ceria catalysts. For the tungsten oxide-modified ceria nanorods, the reduction peak does not appear below 500 °C, and is still small till 800 °C (Fig. 7 (a)). It reveals that the interaction between WO_3 component and CeO_2 support, possibly in the form of W-[O_x]-Ce, is very weak. For the copper-involved samples (CuCe and CuWCe), the related H_2-TPR profiles show multiple peaks in Fig. 7 (a). According to the previous conclusions,[39] the reduction of various copper species supported on ceria includes doped Cu^{2+} ions in the ceria lattice, highly dispersed CuO_x clusters weakly bound to ceria, strongly bound Cu-[O_x]-Ce interacting with the ceria surface and isolated CuO nanoparticles. In this work, we do not find the reduction peaks of crystallized CuO nanoparticles, which typically appears above 200 °C in H_2-TPR.[39] The two major reduction peaks generated for the fresh samples (Fig. 7(a)) can be assigned to the weakly bound CuO_x clusters and strongly bound Cu-[O_x]-Ce species at the low and high temperatures, respectively.[37,38] With an increase in the tungsten content, the intensity of low-temperature reduction is obviously lower, while the intensity of high-temperature reduction becames significantly higher. Table 3 displays that the experimental H_2 consumption rates are significantly higher than the calculated values based on the transformation of Cu^{2+} to Cu^0 only (Table 3). In another word, one copper atom interacts with more than one oxygen atoms, indicating that copper can effectively activate the surface oxygen of ceria support.[37] In order to eliminate the influence of slightly differences on copper concentration in CuCe and CuWCe (see Table 1), we calculated the H_2 consumption rates and normalized the values by the actual Cu amount determined by ICP-AES. From Fig. 7 (b), it is clearly observed that the H_2 consumption rate per copper weight of the CuO_x clusters decreases, while that of the Cu-[O_x]-Ce species increases monotonously with an increase in the tungsten concentration from 0 (CuCe) to 2.0 at% ($CuW_{2.0}Ce$). The addition of more tungsten oxide ($CuW_{3.2}Ce$) does not further promote the reduction of strongly bound Cu-[O_x]-Ce, since few weakly bound CuO_x clusters still exist in $CuW_{2.0}Ce$ (Fig. 7 (a) and Table 3). Therefore, on the basis of the H_2-TPR results, it can be concluded that the major function of introduced tungsten oxide to ceria nanorods is to transfer the weakly bound CuO_x clusters to strongly bound Cu-[O_x]-Ce structure, and finally change the metal-support interaction of copper-ceria catalysts. Interestingly, these two distinguishable copper species do not reflect obvious differences in EXAFS, which is different from the previous findings,[38] indicating that H_2-TPR is a highly effective method to uncover such metal-support interaction.

Table 3
H_2-TPR reduction temperatures (T_R) and H_2 consumption rates (H_2 consp.) of copper catalysts supported on tungsten oxide-modified ceria nanorods.

Sample	T_R (°C)	H_2 consp. (μmol/g)	
		Experimental	Theoretical[c]
CuCe	129[a], 149[b]	1005 (808[a], 197[b])	541
$CuW_{0.4}Ce$	132[a], 147[b]	1050 (666[a], 384[b])	620
$CuW_{2.0}Ce$	146[b]	842[b]	554
$CuW_{3.2}Ce$	153[b]	739[b]	476

[a] For low-temperature reduction.
[b] For high-temperature reduction.
[c] Calculated from complete reduction of Cu^{2+} to Cu^0 theoretically.

As discussed as above, by the aids of multiple characterization techniques, we now have a full view on the structural evolution, as

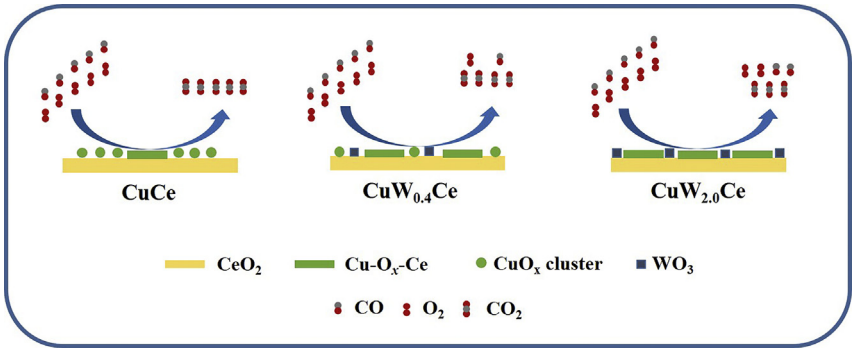

Fig. 8. Schematic demonstration of structural evolution on copper catalysts supported on tungsten oxide-modified ceria nanorods.

well as the structure-activity relationship of the studied copper catalysts supported on tungsten oxide-modified ceria nanorods (Fig. 8). First, the addition of tungsten maintains its W^{6+} valence and does not change the initial Cu^{2+} oxidation state (XANES), which verifies that the electronic structure is not the important factor governing the catalytic performance of copper-ceria in this system. Second, the short-range (up to 0.6 nm) coordination structure around copper center does not show significant modifications after the introduction of tungsten oxide (EXAFS), revealing that the major formation is still Cu–O for both CuCe and CuWCe. Third, the investigated copper species are actually non-crystalline without any observable generation of observable particles (as confirmed by XRD and HRTEM), but both the textural properties (surface area, pore volume and pore size) and the metal-support interaction (H_2-TPR) are clearly modified by the addition of tungsten. In details, the presence of both the weakly bound CuO_x clusters (see the green dots in Fig. 8) and strongly bound Cu-[O_x]-Ce structure (see the green bar in Fig. 8) in CuCe is converted to the creation of strongly bound copper species only in $CuW_{2.0}Ce$. Finally, the effect of tungsten oxide (see the blue square) to ceria is to transfer the CuO_x clusters to Cu-[O_x]-Ce species, and thus impair the catalytic activity of copper-ceria catalysts for the CO oxidation reaction.

4. Conclusions

In summary, small-amount tungsten oxide was introduced into the copper-ceria catalysts by a two-step sequential deposition-precipitation approach. The addition of tungsten in the formation of W^{6+} ion maintains the Cu^{2+} species on the surface of ceria nanorods, and the local coordination structure around copper center is still dominant by the first shell of Cu–O. No crystallized component appears with the introduction of tungsten oxide, but the textural properties of both ceria support and copper-ceria catalysts change. Indeed, the metal-support interaction is significantly modified by the addition of tungsten with the transformation of weakly bound CuO_x clusters to strongly bound Cu-[O_x]-Ce structure. However, the negative effect of tungsten oxide to ceria impaires the catalytic activity of copper-ceria catalyst for the CO oxidation reaction.

References

1. Wang F, Li W, Feng XL, Liu DP, Zhang Y. Decoration of Pt on Cu/Co double-doped CeO_2 nanospheres and their greatly enhanced catalytic activity. *Chem Sci*. 2016;7:1867.
2. Pahalagedara L, Kriz DA, Wasalathanthri N, Weerakkody C, Meng Y, Dissanayake S, et al. Benchmarking of manganese oxide materials with CO oxidation as catalysts for low temperature selective oxidation. *Appl Catal B*. 2017;204:411.
3. Haruta M, Tsubota S, Kobayashi T, Kageyama H, Genet MJ, Delmon B. Low-temperature oxidation of CO over gold supported on TiO_2, α-Fe_2O_3, and Co_3O_4. *J Catal*. 1993;144(1):175.
4. Qiao B, Wang A, Yang X, Allard LF, Jiang Z, Cui Y, et al. Single-atom catalysis of CO oxidation using Pt_1/FeO_x. *Nat Chem*. 2011;3:634.
5. Peterson EJ, DeLaRiva AT, Lin S, Johnson RS, Guo H, Miller JT, et al. Low-temperature carbon monoxide oxidation catalysed by regenerable atomically dispersed palladium on alumina. *Nat Commun*. 2014;5:4885.
6. Wang DS, Li YD. One-pot protocol for Au-based hybrid magnetic nanostructures via a noble-metal-induced reduction process. *J Am Chem Soc*. 2010;132(18):6280.
7. Uzun A, Ortalan V, Hao Y, Browning ND, Gates BC. Nanoclusters of gold on a high-area support: almost uniform nanoclusters imaged by scanning transmission electron microscopy. *ACS Nano*. 2009;3(11):3691.
8. Avgouropoulos G, Ioannides T, Matralis HK, Batista J, Hocevar S. CuO-CeO_2 mixed oxide catalysts for the selective oxidation of carbon monoxide in excess hydrogen. *Catal Lett*. 2001;73(1):33.
9. Li LY, Han WL, Dong F, Zong LY, Tang ZC, Zhang ZY. Controlled pore size of ordered mesoporous Al_2O_3-supported Mn/Cu catalysts for CO oxidation. *Microporous Mesoporous Mater*. 2017;249:1.
10. Kowalik P, Konkol M, Antoniak K, Próchniak W, Wiercioch P. The effect of the precursor ageing on properties of the Cu/ZnO/Al_2O_3 catalyst for low temperature water–gas shift (LT-WGS). *J Mol Catal Chem*. 2014;392(392):127.
11. Schumann J, Eichelbaum M, Lunkenbein T, Thomas N, Galván MCÁ, Schlögl R, et al. Promoting strong metal support interaction: doping ZnO for enhanced activity of Cu/ZnO:M (M = Al, Ga, Mg) catalysts. *ACS Catal*. 2015;5(6):3260.
12. Si R, Flytzani-Stephanopoulos M. Shape and crystal-plane effects of nanoscale ceria on the activity of Au-CeO_2 catalysts for the water-gas shift reaction. *Angew Chem Int Ed*. 2008;47:2884.
13. Du LY, Wang WW, Yan H, Wang X, Jin Z, Song QS, et al. Copper-ceria sheets catalysts: effect of copper species on catalytic activity in CO oxidation reaction. *J Rare Earths*. 2017;35:1186.
14. Eaimsumang S, Wongkasemjit S, Pongstabodee S, Smith SM, Ratanawilai S, Chollacoop N, et al. Effect of synthesis time on morphology of CeO_2 nanoparticles and Au/CeO_2 and their activity in oxidative steam reforming of methanol. *J Rare Earths*. 2019;37:819.
15. Song WY, Jansen APJ, Degirmenci V, Ligthart DAJM, Hensen EJM. A computational study of the mechanism of CO oxidation by a ceria supported surface rhodium oxide layer. *Chem Commun*. 2013;49(37):3851.
16. Liang BL, Duan HM, Su X, Chen XD, Huang YQ, Chen XW, et al. Promoting role of potassium in the reverse water gas shift reaction on Pt/mullite catalyst. *Catal Today*. 2017;281:319.
17. Mudiyanselage K, Senanayake SD, Feria L, Kundu S, Baber AE, Graciani J, et al. Importance of the metal-oxide interface in catalysis: in situ studies of the water-gas shift reaction by ambient-pressure X-ray photoelectron spectroscopy. *Angew Chem Int Ed*. 2013;52(19):5101.
18. Carrettin S, Concepción P, Corma A, Nieto JML, Puntes VF. Nanocrystalline CeO_2 increases the activity of Au for CO oxidation by two orders of magnitude. *Angew Chem Int Ed*. 2004;43(19):2538.
19. Kaspar J, Fornasiero P, Hickey N. Automotive catalytic converters: current status and some perspectives. *Catal Today*. 2003;77:419.
20. Zou HB, Chen SZ, Liu ZL, Lin WM. DRIFTS study of Cu-Zr-Ce-O catalysts for selective CO oxidation. *Int J Hydrogen Energy*. 2009;34:9324.
21. Reddy LH, Reddy GK, Devaiah D, Reddy BM. A rapid microwave-assisted solution combustion synthesis of CuO promoted CeO_2-M_xO_y (M = Zr, La, Pr and Sm) catalysts for CO oxidation. *Appl. Catal. A*. 2012;445:297.
22. Wang J, Deng L, He DD, Lu JC, He SY, He SF, et al. A facile and rapid route to synthesize $CuO_x/Ce_{0.8}Zr_{0.2}O_2$ catalysts with high performance for CO preferential oxidation (CO-PROX). *Int J Hydrogen Energy*. 2015;40:12478.
23. Gu YF, Cai T, Gao XH, Xia HQ, Sun W, Zhao J, et al. Catalytic combustion of chlorinated aromatics over WO_x/CeO_2 catalysts at low temperature. *Appl Catal B*. 2019;248:264.
24. Zhao P, Ye L, Sun ZY, Lo BTW, Woodcock H, Huang C. Entrapped single tungstate site in zeolite for cooperative catalysis of olefin metathesis with brønsted acid site. *J Am Chem Soc*. 2018;140(21):6661.
25. Lwin S, Wachs IE. Olefin metathesis by supported metal oxide catalysts. *ACS Catal*. 2014;4(8):2505.
26. Ishida T, Honma T, Nakada K, Murayama H, Mamba T, Kume K, et al. Pd-catalyzed decarbonylation of furfural: elucidation of support effect on Pd size and catalytic activity using in-situ XAFS. *J Catal*. 2019;374:320.
27. Divins NJ, Casanovas A, Xu W, Senanayake SD, Wiater D, Trovarelli A, et al. The influence of nano-architectured CeO_x supports in RhPd/CeO_2 for the catalytic ethanol steam reforming reaction. *Catal Today*. 2015;253:99.
28. Kugai J, Miller JT, Guo N, Song CS. Oxygen-enhanced water gas shift on ceria-supported Pd-Cu and Pt-Cu bimetallic catalysts. *J Catal*. 2011;277:46.
29. Olmos CM, Chinchilla LE, Villa A, Delgado JJ, Pan HY, Hungria AB, et al. Influence of pretreatment atmospheres on the performance of bimetallic Au-Pd supported on ceria-zirconia mixed oxide catalysts for benzyl alcohol oxidation. *Appl. Catal. A*. 2016;525:145.
30. Guo LW, Du PP, Fu XP, Ma C, Zeng J, Si R, et al. Contributions of distinct gold species to catalytic reactivity for carbon monoxide oxidation. *Nat Commun*. 2016;7:13481.
31. Chen DK, He DD, Lu JC, Zhong LP, Liu F, Liu JP, et al. Investigation of the role of surface lattice oxygen and bulk lattice oxygen migration of cerium-based oxygen carriers: XPS and designed H_2-TPR characterization. *Appl Catal B*. 2017;218:249.
32. Wang WW, Du PP, Zou SH, He HY, Wang RX, Jin Z, et al. Highly dispersed copper oxide clusters as active species in copper-ceria catalyst for preferential oxidation of carbon monoxide. *ACS Catal*. 2015;5(4):2088.
33. Langford JI. Powder pattern programs. *J Appl Crystallogr*. 1971;4:259.
34. Langford JI. The accuracy of cell dimensions determined by Cohen's method of least squares and the systematic indexing of powder data. *J Appl Crystallogr*. 1973;6:190.
35. Shu M, Wei S, Jia CJ, Wang DL, Si R. Effect of nickel oxide doping to ceria-supported gold catalyst for CO oxidation and water-gas shift reactions. *J Catal*. 2018;8(12):584.
36. Wang X, Du LY, Du M, Ma C, Zeng J, Jia CJ, et al. Catalytically active ceria-supported cobalt-manganese oxide nanocatalysts for oxidation of carbon monoxide. *Phys Chem Chem Phys*. 2017;19:14533.
37. Du PP, Wang WW, Jia CJ, Song QS, Huang YY, Si R. Effect of strongly bound copper species in copper-ceria catalyst for preferential oxidation of carbon monoxide. *Appl Catal Gen*. 2016;518:87.
38. Wang WW, Yu WZ, Du PP, Xu H, Jin Z, Si R, et al. Crystal plane effect of ceria on supported copper oxide cluster catalyst for CO oxidation: importance of metal-support interaction. *ACS Catal*. 2017;7(2):1313.
39. Si R, Raitano J, Yi N, Zhang L, Chan SW, Flytzani-Stephanopoulos M. Structure sensitivity of the low-temperature water-gas shift reaction on Cu–CeO_2 catalysts. *Catal Today*. 2012;180:68.